THE JOURNAL OF BIOLOGICAL CHEMISTRY VOL. 283, NO. 45, pp. 30668–30676, November 7, 2008

Homomeric and Heteromeric Assembly of KCNQ (Kv7) K^+ Channels Assayed by Total Internal Reflection Fluorescence/Fluorescence Resonance Energy Transfer and Patch Clamp Analysis*[S]

Received for publication, July 9, 2008, and in revised form, August 28, 2008 Published, JBC Papers in Press, September 11, 2008, DOI 10.1074/jbc.M805216200

Manjot Bal, Jie Zhang, Oleg Zaika, Ciria C. Hernandez, and Mark S. Shapiro[1]

From the Department of Physiology, University of Texas Health Science Center, San Antonio, Texas 78229

M-type K^+ channels, consisting of KCNQ1–5 (Kv7.1–7.5) subunits, form a variety of homomeric and heteromeric channels. Whereas all the subunits can assemble into homomeric channels, the ability of the subunits to assemble into heteromultimers is highly variable. KCNQ3 is widely thought to co-assemble with several other KCNQ subtypes, whereas KCNQ1 and KCNQ2 do not. However, the existence of other subunit assemblies is not well studied. To systematically explore the heteromeric assembly of KCNQ channels in individual living cells, we performed fluorescence resonance energy transfer (FRET) between cyan fluorescent protein- and yellow fluorescent protein-tagged KCNQ subunits expressed in Chinese hamster ovary cells under total internal reflection fluorescence microscopy in which excitation light only penetrates several hundred nanometers into the cell, thus isolating membrane events. We found significant FRET between homomeric subunits as expected from their functional expression in heterologous expression systems. Also as expected from previous work, robust FRET was observed between KCNQ2 and KCNQ3. KCNQ3 and KCNQ4 also showed substantial FRET as did KCNQ4 and KCNQ5. To determine functional assembly of KCNQ4/KCNQ5 heteromers, we performed two types of experiments. In the first, we constructed a mutant tetraethylammonium ion-sensitive KCNQ4 subunit and tested its assembly with KCNQ5 by patch clamp analysis of the tetraethylammonium ion sensitivity of the resulting current; however, those data were not conclusive. In the second, we co-expressed a KCNQ4 (G285S) pore mutant with KCNQ5 and found the former to act as a dominant negative, suggesting co-assembly of the two types of subunits. These data confirm that among the allowed assembly conformations are KCNQ3/4 and KCNQ4/5 heteromers.

The KCNQ (Kv7) family of voltage-gated channels underlie a number of important K^+ currents throughout the body, including the M current of neurons produced by the homomeric and heteromeric assembly of KCNQ2, KCNQ3, and KCNQ5 (1–7). KCNQ4 makes homomeric K^+ channels important for K^+ transport primarily in the inner ear (8, 9), whereas KCNQ1 assembles with KCNE β-subunits to form several important currents in heart, ear, and epithelia (10, 11). The understanding of the different subunit compositions of KCNQ channels is important because such compositions affect the properties of the channels. Thus, expression of KCNQ2 and KCNQ3 individually yields only small whole-cell currents, whereas their co-expression yields heteromeric currents 10-fold larger (5, 12–16). Homomeric KCNQ2, -4, and -5 channels are sensitive to Ca^{2+}/calmodulin, whereas KCNQ1 and KCNQ3 are not (17). Finally KCNQ1 and KCNQ2 subunits in particular have been shown to be modulated by phosphorylation by protein kinases A and C, respectively, via complexes assembled by the scaffolding proteins yotiao and AKAP79/150 (18–21). Therefore, it is expected that the inclusion of these different subunits in the channel tetramer should confer specific properties characteristic of each subunit to the functional channels.

Previous work broadly indicates KCNQ3 to be the most promiscuous KCNQ subunit, assembling with KCNQ2 to make the classic "M channel" of sympathetic ganglia (1, 4, 5, 13, 14) and KCNQ5 to produce KCNQ3/5 heteromeric channels when expressed in heterologous systems and likely also existing as such in brain regions as well (3, 22, 23). Although co-expression data in oocytes suggest that KCNQ3 and KCNQ4 might co-assemble (8), that conclusion still seems tentative. On the other hand, KCNQ2 has been clearly shown to not assemble with any other type subunit besides KCNQ3 (3, 8), and KCNQ1, although robustly assembling with the family of KCNE β-subunits to form a variety of heteromeric channels with different properties, does not assemble with any of the other KCNQ2–5 subunits (3, 8, 16, 23, 24). The possibility that KCNQ4 and KCNQ5 might co-assemble to form functional channels is as yet unexplored.

In this study, we set about to systematically investigate the assembly of KCNQ1–5 subunits in mammalian cells using fluorescence resonance energy transfer (FRET).[2] The FRET technique allows the investigation of protein/protein interactions in

* This work was supported, in whole or in part, by National Institutes of Health Grant R01 NS043394 (to M. S. S.). This work was also supported by an American Heart Association-Texas affiliate grant-in-aid (to M. S. S.). The costs of publication of this article were defrayed in part by the payment of page charges. This article must therefore be hereby marked "*advertisement*" in accordance with 18 U.S.C. Section 1734 solely to indicate this fact.

[S] The on-line version of this article (available at http://www.jbc.org) contains supplemental Fig. S1.

[1] To whom correspondence should be addressed: Dept. of Physiology, MS 7756, University of Texas Health Science Center, 7703 Floyd Curl Dr., San Antonio, TX 78229. Tel.: 210-567-4328; Fax: 210-567-4410; E-mail: shapirom@uthscsa.edu.

[2] The abbreviations used are: FRET, fluorescence resonance energy transfer; YFP, yellow fluorescent protein; CFP, cyan fluorescent protein; TIRF, total internal reflection fluorescence; CHO, Chinese hamster ovary; TEA, tetraethylammonium ion.

individual cells (25, 26) and has proven to be a robust technique for the investigation of channel composition and stoichiometry (27–30). Furthermore, experiments were performed on individual living cells imaged under total internal reflection fluorescence (TIRF) microscopy, in which the illumination penetrates only to a depth of <400 nm into the cells (31), isolating mostly membrane interactions. Thus, our TIRF/FRET paradigm allowed us to assay the interactions of subunits assembled only as channels at the membrane where they are functional, ignoring any channel assemblies in the endoplasmic reticulum or other internal organelles where they would be much less relevant to cellular function. We also performed electrophysiology to test the functional behavior of putative subunit assemblies identified in our TIRF/FRET experiments. We found that KCNQ4 assembles not only as homomers but also as heteromers with KCNQ3 and KCNQ5, raising the possibility that heteromeric KCNQ3/4 and KCNQ4/5 channels exist in neurons, further diversifying the portfolio of allowed KCNQ subunit compositions that likely enrich the repertoire of nervous system function.

EXPERIMENTAL PROCEDURES

cDNA Constructs—KCNQ1 (human), KCNQ2 (human), KCNQ3 (rat), KCNQ4 (human), and KCNQ5 (human) (GenBank™ accession numbers NM000218, AF110020, AF091247, AF105202, and AF249278, respectively) were kindly given to us by Michael Sanguinetti (KCNQ1; University of Utah, Salt Lake City, UT), David McKinnon (KCNQ2 and KCNQ3; State University of New York, Stony Brook, NY), Thomas Jentsch (KCNQ4; Zentrum fur Molekulare Neurobiologie, Hamburg, Germany), and Klaus Steinmeyer (KCNQ5; Aventis Pharma, Frankfurt am Main, Germany). Plasmids were subcloned into pECFP-N1 or pEYFP-N1 vectors (Clontech) using standard techniques. The membrane-localized cyan fluorescent protein (CFP)-yellow fluorescent protein (YFP) tandem construct (Rho-pYC) was kindly given to us by Paul Slesinger (Salk Institute, La Jolla, CA). It consists of the carboxyl-terminal prenylation site of Rho (RQKKRRGCLLL) appended to the carboxyl terminus of a YFP-CFP fusion (32). The KCNQ4 (T290Y) and KCNQ4 (G285S) mutants used in this study were generated by QuikChange PCR mutagenesis according to the manufacturer's instructions.

Cell Culture and cDNA Transfections—Chinese hamster ovary (CHO) cells were grown in 100-mm tissue culture dishes (Falcon) in Dulbecco's modified Eagle's medium with 10% heat-inactivated fetal bovine serum plus 0.1% penicillin and streptomycin in a humidified incubator at 37 °C (5% CO_2) and passaged about every 4 days. Cells were discarded after about 30 passages. For TIRF/FRET experiments, cells were first passaged onto 35-mm plastic tissue culture dishes and transfected 24 h later with Polyfect reagent (Qiagen) according to the manufacturer's instructions and as described previously (33). The next day, cells were plated onto poly-L-lysine-coated glass-bottomed 35-mm tissue culture dishes (MatTek, Ashland, MA), and experiments were performed over the following 1–2 days.

TIRF Microscopy—Fluorescence emission from enhanced CFP-tagged or enhanced YFP-tagged KCNQ1–5 channels were collected from transiently transfected CHO cells at room temperature using TIRF (also called evanescent field) microscopy. TIRF generates an evanescent field that declines exponentially with increasing distance from the interface between the cover glass and the cytoplasm, illuminating only a thin section (~400 nm) of the cell very near the cover glass, including the plasma membrane (31). All TIRF experiments were performed in the total internal reflection fluorescence microscopy core facility housed within the Department of Physiology at the University of Texas Health Science Center, San Antonio, TX. Fluorescence emissions were collected using an inverted TE2000 microscope with through-the-lens (prismless) TIRF imaging (Nikon). This system is equipped with a vibration isolation system (Technical Manufacturing Corp.) to minimize drift and noise. Samples were viewed through a plan-Apo TIRF 60× oil immersion high resolution (1.45 numerical aperture) TIRF objective. Coupled to the microscope is a laser light delivery system (Prairie Technologies) consisting of a 40-milliwatt argon laser outputting 488 and 514 nm lines and a 442-nm diode-pumped solid-state laser. The excitation light was selected with an acoustic optical tunable filter controlled by MetaMorph software running on a PC. CFP and YFP emissions were simultaneously collected using the Dual-View chip splitter (Optical Insights) equipped with a filter cube containing HQ 470 nm/30 nm and HQ 550 nm/30 nm emission filters for CFP and YFP emission, respectively, and a 505-nm dichroic mirror for separation of emission wavelengths. In this configuration, the microscope uses only a dual bandpass TIRF dichroic mirror to separate the excitation and emission light with no excitation filters used. The TIRF angle was adjusted by eye to give the signature TIRF illumination to the experimental chamber. Fluorescence images were collected and processed with a 16-bit, cooled charge-coupled device camera (Cascade 512F, Roper Scientific Inc.) interfaced to a PC running MetaMorph software. This camera uses a front-illuminated electron-multiplying charge-coupled device with on-chip multiplication gain. Images were collected (200–600-ms exposure time) immediately before and after photobleaching. Images were not binned or filtered; pixel size corresponded to a square of 122 × 122 nm.

Fluorescence Resonance Energy Transfer—We used the acceptor photobleaching method of evaluating FRET efficiency in which the emission of the donor fluorophore is compared before and after photobleaching of the acceptor (34). YFP photobleaching was performed using the 100-watt mercury lamp of the microscope using a standard YFP filter cube. All image acquisition was computer-controlled by MetaMorph software. We found that a 5–7-min excitation by the mercury lamp using the YFP cube is sufficient to photobleach >80% of the YFP fluorophores yet results in negligible photobleaching of the CFP fluorophores. The following protocol was used. The medium in the glass-bottomed dishes was exchanged with Ringer's solution that contained 160 mM NaCl, 5 mM KCl, 1 mM $MgCl_2$, 2 mM $CaCl_2$, 10 mM HEPES, pH 7.4 with NaOH. Cells were first examined using the mercury lamp and standard CFP or YFP filter cubes to find a suitable cell robustly expressing both CFP- and YFP-tagged channels. Under TIRF illumination, the focal plane used is critical and was adjusted if necessary immediately before each image acquisition to obtain a sharp TIRF image. The focusing and cell-centering protocol resulted

in CFP photobleaching of <1%. TIRF images using 442 and 514 nm laser lines were acquired before and after photobleaching of the YFP fluorophores. %FRET was calculated as the percent increase in CFP emission after YFP photobleaching by using the formula $\%FRET = (CFP_{post} - CFP_{pre}/CFP_{pre}) \times 100$ where CFP_{post} is CFP emission after YFP photobleaching and CFP_{pre} is CFP emission before YFP photobleaching. The %FRET was calculated by drawing regions of interest around the entire area of the cell and subtracting the background in a cell-free region for each image.

Perforated Patch Electrophysiology—CHO cells heterologously expressed with KCNQ channels were studied as described previously (33). Enhanced green fluorescent protein was used as a reporter for successful transfection. Standard bathing and pipette solutions were used (15). To quantify the KCNQ current amplitude (I_{KCNQ}), two methods were used. For the tetraethylammonium ion (TEA) block experiments (Fig. 4) in which the currents were fairly large, I_{KCNQ} was defined as the amplitude of the current at the holding potential of 0 mV. For the pore mutant experiments (Fig. 5) in which there were currents of sharply variable amplitude, I_{KCNQ} was defined as the time-dependent relaxation at −60 mV. This was measured by subtracting the current amplitude at the end of the pulse to −60 mV from the amplitude 5 ms after the start (after the capacity transient had subsided) (15).

Hill Equation Fitting—The homomeric data in Fig. 4 were fit by Hill equations of the form $\%Block = 100/(1 + (K_{½}/[TEA])^n)$ where $K_{½}$ is the concentration of TEA that yields half-block and n is the Hill coefficient. The co-expression data were fit either by a double Hill equation or by the sum of five Hill equations with the only free parameter being the probability of any one subunit being a KCNQ4 (T290Y) *versus* a KCNQ5 as described in the text. For the latter, the $K_{½}$ values used were 1.28, 3.10, 7.5, 18.13, and 43.9 mM for channels with KCNQ4 (T290Y):KCNQ5 stoichiometries of 4:0, 3:1, 2:2, 1:3, and 0:4, respectively. For equal abundance of subunits between the two, the binomial equation predicts relative populations of 1:4:6:4:1, respectively, where we assumed that two like subunits being adjacent in the tetramer had the same effect as them being diagonally opposed. The two kinds of fits yielded the probability of any subunit being a KCNQ4 (T290Y) to be 0.63 in both cases.

Statistics—All values are reported as mean ± S.E. Statistical significance was assessed using a t test. The results obtained were considered significant at $p < 0.05$.

RESULTS

Homomeric Interaction of KCNQ Subunits Assayed by TIRF/FRET

Although a number of *in vitro* techniques exist to assay protein/protein interactions, we wished to investigate intersubunit interactions in the native intracellular environment of living cells. Thus, we chose the technique of FRET in which interactions are monitored as non-radiative energy transfer between two fluorophores for which the emission spectrum of one (the "donor") overlaps with the excitation spectrum of the other (the "acceptor"). FRET has the very steep dependence on distance between the fluorophores with an efficiency that falls off with the sixth power of the distance between the fluorophores relative to the Förster distance (which is typically ~50 Å). If a pair of fluorophores is attached to two proteins, then only if they are in very close proximity, such as when bound together, will there be appreciable FRET (26). We used the widely used FRET pair of enhanced CFP and enhanced YFP. FRET was measured in CHO cells transiently transfected with the CFP- and YFP-tagged channels. Moreover the experiments were performed under TIRF microscopy (31). TIRF illumination involves directing a laser beam at the interface between two transparent media of differing refractive indices at a glancing angle. By the laws of optics, at an angle greater than the critical angle determined by the ratio of the two refractive indices, the light beam is not primarily transmitted to the second medium but is instead reflected; however, not all the light energy is reflected; a component penetrates into the second medium as an "evanescent wave" that decays exponentially in intensity over a distance of only several hundred nanometers. In this case, the two refractive media are the glass coverslip and the cytoplasm. Thus, we can selectively excite only fluorophores located within ~400 nm of the plasma membrane of the cell by directing laser light at such a glancing angle through a special TIRF objective (35).

Our recent work indicates that our TIRF setup well isolates membrane events with only a minor contribution from molecules localized to the endoplasmic reticulum. In one series of experiments, we compared the emission under wide field or TIRF illumination from membrane-localized green fluorescent protein or cytoplasmic red fluorescent protein (dsRed2) constructs. Whereas the emission from both was strong under wide field illumination, only emission from the membrane-localized green fluorescent protein was detected under TIRF with none from dsRed2 (36). In the other series of tests, we compared the emission under wide field and TIRF illumination from two different sets of plasma membrane or endoplasmic reticulum-resident proteins. Again both sets of proteins were strongly detected under wide field illumination, but only the plasma membrane proteins were significantly detected under TIRF conditions (37).

We first performed positive and negative control experiments to determine the dynamic range feasible with our technique. For the former, we used as a positive control the RhopYC construct that consists of a membrane-targeted fusion of CFP and YFP (Fig. 1, *A* and *C*). FRET efficiency was quantified as the fractional increase in CFP emission following selective photobleaching of YFP using the formula as described under "Experimental Procedures." The FRET efficiency for this construct was 26.0 ± 1.2%, and the photobleach of YFP was 85.6 ± 1.2% ($n = 18$). For the latter, we used CFP-tagged KCNQ2 and YFP-tagged epithelial Na^+ channel α-subunit (ENaC) as these two membrane proteins are not known to interact with each other (Fig. 1, *B* and *C*). The FRET efficiency between these two constructs was 1.2 ± 0.6%, and the photobleach of YFP was 79.8 ± 3.4% ($n = 26$). Being satisfied that the method was robust for our requirements we performed further FRET experiments. To demonstrate subunit/subunit interactions of KCNQ channels, we constructed carboxyl-terminal fusion constructs of KCNQ1–5 channels tagged with CFP or YFP. To monitor homomeric assembly of KCNQ1–5 channels, CFP- and YFP-

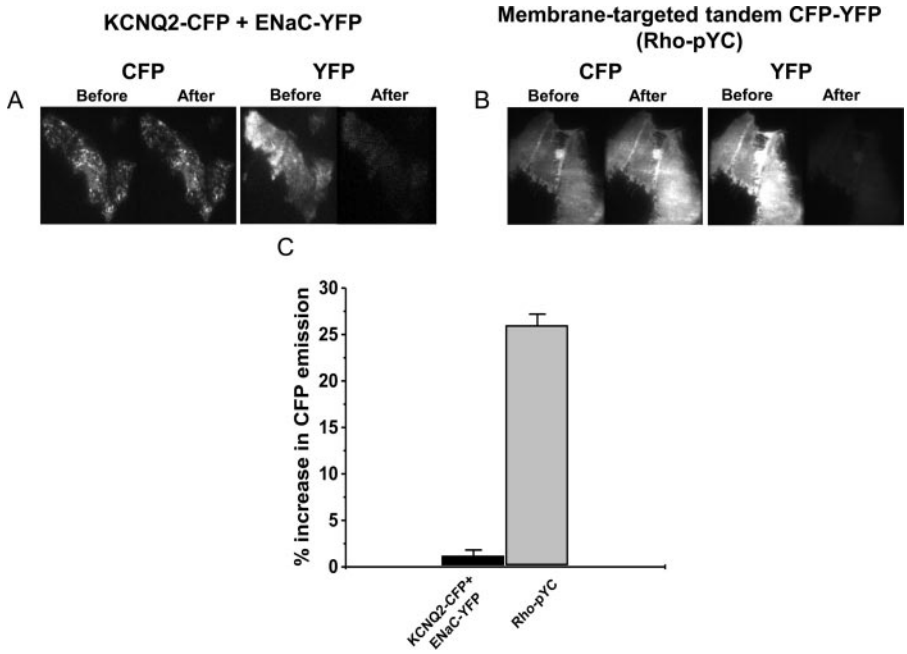

FIGURE 1. **Positive and negative controls for FRET under TIRF microscopy.** *A*, images of CHO cells expressing CFP-tagged KCNQ2 and YFP-tagged ENaC. Panels show CFP (*left*) and YFP (*right*) emissions before and after selective photobleaching of YFP. Note the lack of increase in CFP emission after YFP photobleaching, indicating minimal FRET. *B*, CHO cells expressing a membrane-targeted tandem construct of CFP and YFP (Rho-pYC) before and after selective photobleaching of YFP. Panels show CFP (*left*) and YFP (*right*) emissions before and after selective photobleaching of YFP. The strong increase in CFP emission after YFP photobleaching indicates robust FRET. *C*, *bars* show summarized FRET efficiency data calculated as the percent increase in CFP emission after YFP photobleaching. *Error bars* show standard errors.

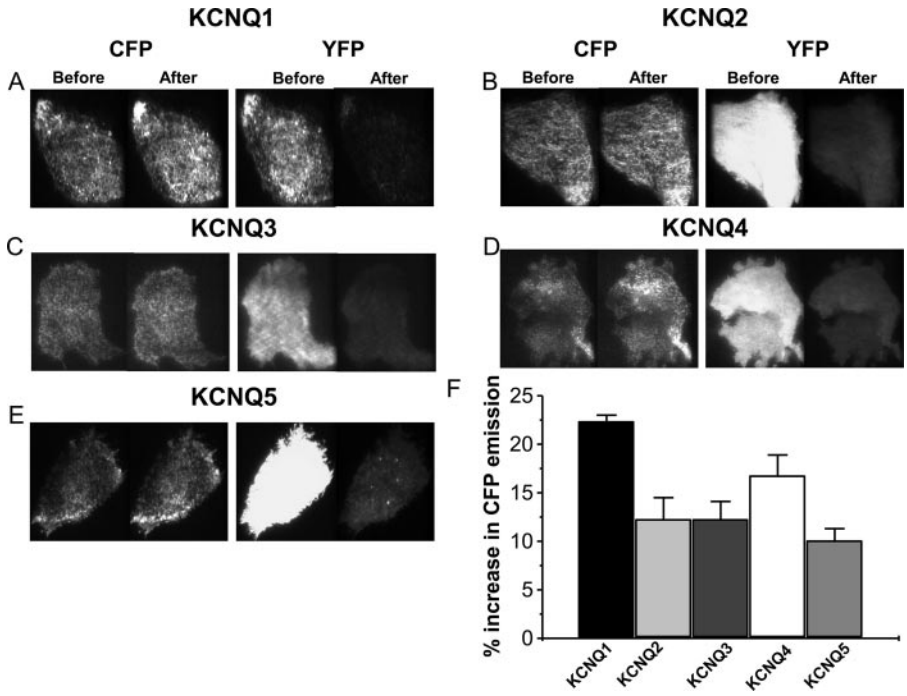

FIGURE 2. **Homomeric interaction between KCNQ1–5 subunits assayed by TIRF/FRET.** CHO cells were co-transfected with homomeric CFP- and YFP-tagged KCNQ1 (*A*), KCNQ2 (*B*), KCNQ3 (*C*), KCNQ4 (*D*), or KCNQ5 (*E*) subunits. Panels show CFP (*left*) and YFP (*right*) emissions before and after selective photobleaching of YFP. *F*, *bars* show summarized FRET efficiency data calculated as the percent increase in CFP emission after YFP photobleaching. *Error bars* show standard errors.

tagged versions of the same subunit were co-transfected (using equal amounts of cDNA) in CHO cells, and the FRET was assayed between them (Fig. 2). For each subunit type, there was strong FRET with that of KCNQ1 being the strongest and KCNQ5 being slightly weaker. These data are summarized in Fig. 2*F*. For KCNQ1, KCNQ2, KCNQ3, KCNQ4, and KCNQ5, the FRET efficiencies were 22.4 ± 0.6% (n = 17), 12.3 ± 2.2% (n = 9), 12.3 ± 1.7% (n = 6), 16.8 ± 2.1% (n = 10), and 10.1 ± 1.2% (n = 10), respectively. The YFP photobleach in these experiments was 80.0 ± 0.7, 82.0 ± 4.0, 82.8 ± 2.8, 80.6 ± 1.7, and 84.6 ± 1.2%, respectively. The FRET results are in accord with the robust currents from KCNQ1, KCNQ4, and KCNQ5 homomeric channels widely reported in the literature and also indicate that the smaller currents known to be produced by KCNQ2 and KCNQ3 homomers are not the result of impaired homomeric assembly of KCNQ2 or KCNQ3 subunits (see "Discussion").

Heteromeric Interaction of KCNQ1–5 Channel Subunits

We then used our TIRF/FRET technique to probe the allowed heteromeric assembly of KCNQ1–5 subunits. We were particularly interested in the allowed assembly of KCNQ4 with KCNQ3 or KCNQ5, which has not been well described. In these experiments, we exploited as positive and negative controls the accepted heteromeric assembly of KCNQ2/3 subunits (4, 5, 14, 38, 39) and the reported lack of assembly of KCNQ1 with KCNQ4 (8) and of KCNQ2 with KCNQ5 (3). CHO cells were co-transfected with five different combinations of CFP- or YFP-tagged KCNQ1–5 subunits, and their assembly was evaluated by the resulting FRET efficiency (Fig. 3). Neither co-expression of CFP-tagged KCNQ1 + YFP-tagged KCNQ4 (Fig. 3*A*) nor CFP-tagged KCNQ2 + YFP-tagged KCNQ5 (Fig. 3*B*) yielded FRET that was significantly larger than the CFP-tagged KCNQ2 + YFP-tagged ENaC control. Thus, CHO cells transfected with CFP-tagged KCNQ1 + YFP-tagged KCNQ4 or CFP-tagged KCNQ2 + YFP-tagged KCNQ5 displayed FRET efficiencies of 4.1 ± 2.5% (n = 12) and 3.7 ± 2.9% (n = 16), and the photobleach of YFP was 90.2 ± 0.6 and

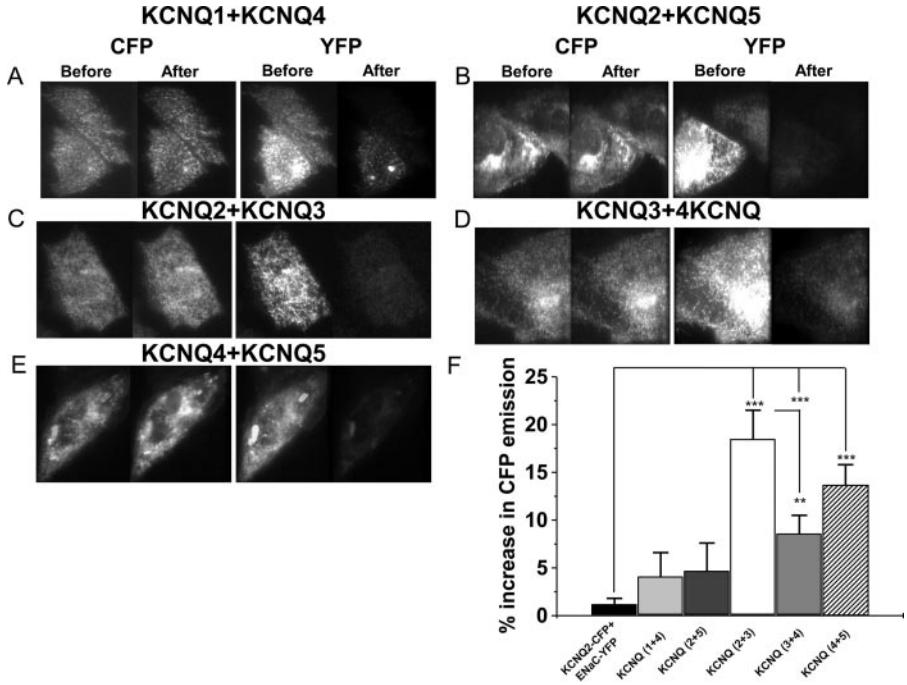

FIGURE 3. **Heteromeric interaction between KCNQ subunits assayed by TIRF/FRET.** CHO cells were co-transfected with CFP-tagged KCNQ1 + YFP-tagged KCNQ4 (*A*), CFP-tagged KCNQ2 + YFP-tagged KCNQ5 (*B*), KCNQ2-CFP and KCNQ3-YFP (*C*), KCNQ3-CFP and KCNQ4-YFP (*D*), or CFP-tagged KCNQ4 and YFP-tagged KCNQ5 (*E*). The panels show CFP and YFP emission images before and after selective photobleaching of YFP. *F*, *bars* indicate the summarized FRET efficiency data calculated as the percent increase in CFP emission after YFP photobleaching (**, $p < 0.01$; ***, $p < 0.001$). *Error bars* show standard errors.

89.4 ± 2.6%, respectively (Fig. 3*F*). These data suggest the lack of interaction between these subunit pairs in accord with their lack of assembly. On the other hand, FRET measured between CFP-tagged KCNQ2 and YFP-tagged KCNQ3 was robust. The FRET efficiency was 18.5 ± 2.9%, and the photobleach of YFP was 81.4 ± 4.4% ($n = 9$) (Fig. 3, *C* and *F*) in accord with their strong interaction and robust assembly shown by patch clamp experiments. We then assayed the interaction of KCNQ4 with either KCNQ3 or KCNQ5. CHO cells co-expressing CFP-tagged KCNQ3 and YFP-tagged KCNQ4 displayed a significant FRET, which was 10.5 ± 1.2%, and the photobleach of YFP was 87.7 ± 1.8% ($n = 8$) (Fig. 3, *D* and *F*). Similarly CHO cells co-expressing CFP-tagged KCNQ4 and YFP-tagged KCNQ5 also displayed significant FRET, which was 13.7 ± 2.1%, and the photobleach of YFP was 83.2 ± 1.1% ($n = 10$) (Fig. 3, *E* and *F*). These data indicate that KCNQ3 and KCNQ4 interact, consistent with functional assembly (8). They also suggest that KCNQ4 and KCNQ5 also interact, leading to the possibility that they form functional heteromeric channels. The FRET between KCNQ3 and KCNQ4, although significant, was less than that between KCNQ2 and KCNQ3, possibly suggesting a weaker assembly efficiency of the former relative to the latter.

Do KCNQ4 and KCNQ5 Co-assemble to Form Functional Heteromers?

TEA Block—Given the TIRF/FRET evidence of interaction between KCNQ4 and KCNQ5, we then proceeded to test their functional assembly by mutagenesis and patch clamp analysis of two types. The first method attempted to use the analysis of channel block by extracellular TEA. The widely divergent sensitivity of KCNQ2 and KCNQ3 subunits to TEA has been used to demonstrate the functional assembly of these subunits (4, 40). Thus, KCNQ2 is highly TEA-sensitive with an IC_{50} of 0.1–0.3 mM, KCNQ3 is very TEA-insensitive with an IC_{50} of >100 mM, and native M current or KCNQ2/3 heteromers have an intermediate TEA sensitivity with an IC_{50} of 5–10 mM (4, 5, 40). The high TEA sensitivity of KCNQ2 localizes to Tyr-284, corresponding to Tyr-449 in Shaker channels that confers high TEA sensitivity (41, 42). KCNQ4 and KCNQ5 have a threonine in that position and are consequently both much less TEA-sensitive (3, 40). To use TEA block to demonstrate functional assembly in this way, we thus made the KCNQ4 (T290Y) point mutant, which we reasoned would produce a KCNQ4 channel with relatively high sensitivity to extracellular TEA.

CHO cells were transfected with either wild-type KCNQ4, KCNQ5, KCNQ4 (T290Y), or KCNQ4 (T290Y) + KCNQ5, and the sensitivities to external TEA of the resulting currents were analyzed under perforated patch electrophysiology. Fig. 4*A* shows representative current traces from these experiments, and the summarized data are shown in Fig. 4*B* plotted as %Block *versus* [TEA]. For wild-type KCNQ4, KCNQ5, and KCNQ4 (T290Y), the data were fit by a simple Hill equation. We assumed that all the channels would be fully blocked at infinite [TEA] and fully unblocked at zero [TEA] and so constrained the Hill curves to have a maximum of 100% and a minimum of 0. Furthermore because each channel has only one pore and thus one TEA binding site, we constrained the Hill coefficient to be unity, which yielded excellent fits for all except wild-type KCNQ4 (see below). The T290Y mutation did indeed strongly increase the sensitivity of the KCNQ4 channel to external TEA by approximately 40-fold. For wild-type KCNQ4, the Hill curve with a coefficient of unity did not fit the data well likely because we cannot measure the block at sufficiently high concentrations as was the case previously for KCNQ3 (4). Thus, the unconstrained fit yielded an IC_{50} of 52.0 ± 3.0 mM ($n = 15$) with an n_H of 0.62 ± 0.02, both of which we take to be estimates. For KCNQ4 (T290Y), the IC_{50} was 1.3 ± 0.2 mM ($n = 11$). For KCNQ5, the IC_{50} value was 43.9 ± 0.4 mM ($n = 12$), very similar to wild-type KCNQ4 and to that reported previously for KCNQ5 (3). Interestingly our value for the IC_{50} of TEA block for wild-type KCNQ4 is some 17-fold higher than that described previously (40) but seems reasonable given its similarity to that of KCNQ3 and KCNQ5 and the common threonine at that position among those channels.

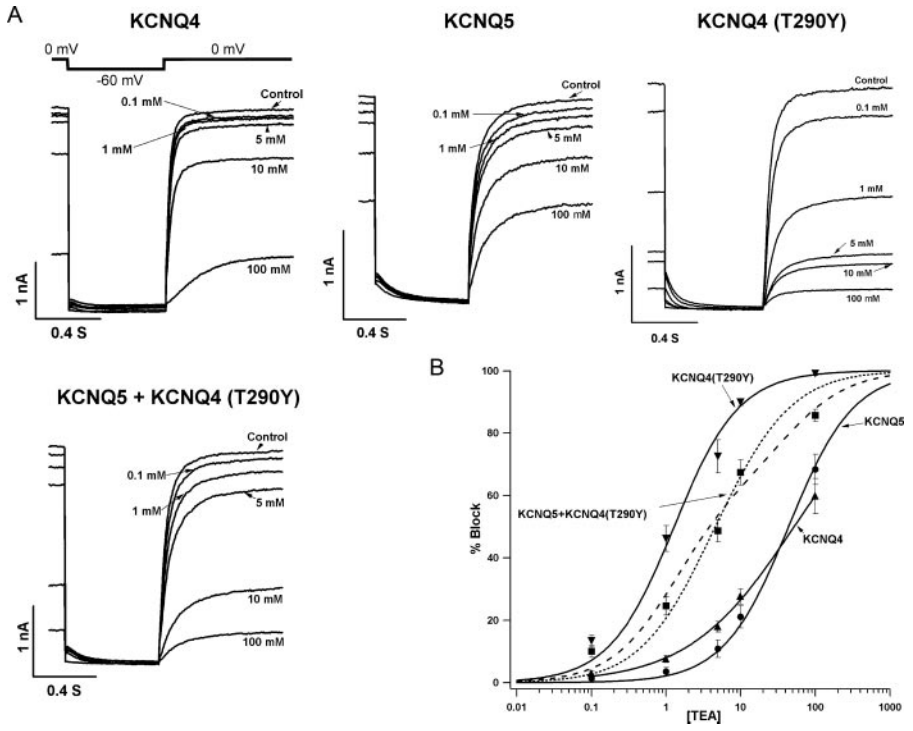

FIGURE 4. **TEA dose-response relationship for KCNQ4, KCNQ4 (T290Y), and KCNQ5 channels.** CHO cells were transfected with the indicated subunits, and the current was studied under perforated patch voltage clamp. *A*, representative currents from the indicated transfections with zero (control) or the indicated concentrations of TEA in the bath. The voltage protocol used is depicted in the *inset*. *B*, plotted are the summarized data of the percent block of the indicated current as a function of [TEA]. The KCNQ current was measured as the amplitude of the holding current at 0 mV. The data for wild-type KCNQ4, KCNQ5, and KCNQ4 (T290Y) were fit by single Hill equations (see "Experimental Procedures"). The data from co-expression of KCNQ4 (T290Y) + KCNQ5 were fit either by a double Hill equation with the $K_{1/2}$ values taken from the fits of the corresponding homomeric currents (*dashed line*) or by the sum of five Hill equations corresponding to the five populations of channels predicted by the binomial relation with the $K_{1/2}$ for each population calculated according to energy additivity of each subunit (see text) and the $K_{1/2}$ values for KCNQ4 (T290Y) and KCNQ5 taken from the fits of the corresponding homomeric currents (*dotted line*). For all the fits, except KCNQ4, the minimum and maximum were constrained to be 0 and 100%, respectively, and the Hill coefficient was constrained to be unity.

When KCNQ4 (T290Y) and KCNQ5 subunits were co-transfected in CHO cells, currents were produced with TEA sensitivity intermediate between that of the two homomers. We then considered the two possibilities that could underlie the intermediate sensitivity. The first is that the two types of subunits do not co-assemble. In that case, two populations of homomeric channels would be produced with a 34-fold difference in IC_{50} values. To see how well that case fit the data, the points were fit by a double Hill equation with the IC_{50} values taken from the fits of the KCNQ4 (T290Y) and KCNQ5 homomeric data, and the only free parameter was the relative abundance of the two types of subunit. The best fit is shown as a *dashed line* in Fig. 4*B*. The other case is that the two types of subunits do co-assemble. In that case, if assembly of expressed subunits into functional tetramers is random, then co-expression of KCNQ4 (T290Y) and KCNQ5 should result in five classes of tetramers containing from zero to four subunits of each type with a distribution governed by the binomial distribution. For the well studied Shaker K^+ channels, external TEA block is at the outer mouth of the selectivity filter, at a site coordinated by all four subunits, with an overall blocking affinity for heteromeric channels that accords with the geometric mean of the affinities of each subunit (4, 41, 43, 44). Thus, we attempted to fit the dose-response relation for co-expressed KCNQ4 (T290Y) + KCNQ5 by the sum of five Hill equations, assuming the binomial distribution and energy additivity of each subunit. The IC_{50} values for each of the five predicted populations were calculated from the IC_{50} values taken from the fits of the KCNQ4 (T290Y) and KCNQ5 homomers, and the only free parameter was the relative abundance of the two types of subunits. The best fit of the data for this case is shown in Fig. 4*B* as the *dotted line*. Unfortunately we judged neither fit to be superior to the other, and we conclude that we cannot demonstrate functional co-assembly of the two subunits using this approach. Thus, whereas superficial inspection of the intermediate TEA sensitivity could lead one to use these data to demonstrate co-assembly of the two subunits, quantitative analysis suggests otherwise. Therefore, we pursued the alternative, and actually simpler, approach of a dominant-negative pore mutant.

Dominant-Negative KCNQ4 Pore Mutant—Because the selectivity filters from all four subunits in the tetramer must be functional for the channel to conduct ions, we can use a non-functional pore mutant as a dominant negative to indicate subunit assembly. This method assumes that parts of the channel outside of the selectivity filter coordinate assembly of the subunits and that one or more subunits with non-functional pores incorporated into the tetramer will preclude ionic permeation. This analysis has been used previously for KCNQ3–5 subunits (3, 8). We examined the effect of the KCNQ4 (G285S) mutation that is naturally found in patients suffering from dominant deafness. This mutant channel does not yield any detectable currents when expressed in *Xenopus* oocytes (8), and so we could use it as a tool for detection of KCNQ4 and KCNQ5 heteromeric assembly. Fig. 5*A* shows currents from transfection in CHO cells of KCNQ5, KCNQ4 (G285S), and KCNQ5 + KCNQ4 (G285S). As a control, we also examined currents resulting from transfection of wild-type KCNQ4 either alone or together with KCNQ4 (G285S) (Fig. 5*B*). The current densities from these cells, quantified as the time-dependent relaxation at −60 mV, are summarized in Fig. 5*C*. Cells transfected with wild-type KCNQ4 yielded robust currents (13.3 ± 0.6 pA/picofarad, $n = 9$), whereas cells transfected with KCNQ4 (G285S) yielded no detectable currents ($n = 16$). We verified that the lack of currents from the pore mutant was not because of lack of expression of the subunits at the membrane by performing TIRF imaging, which revealed fluorescence from CFP-tagged wild-

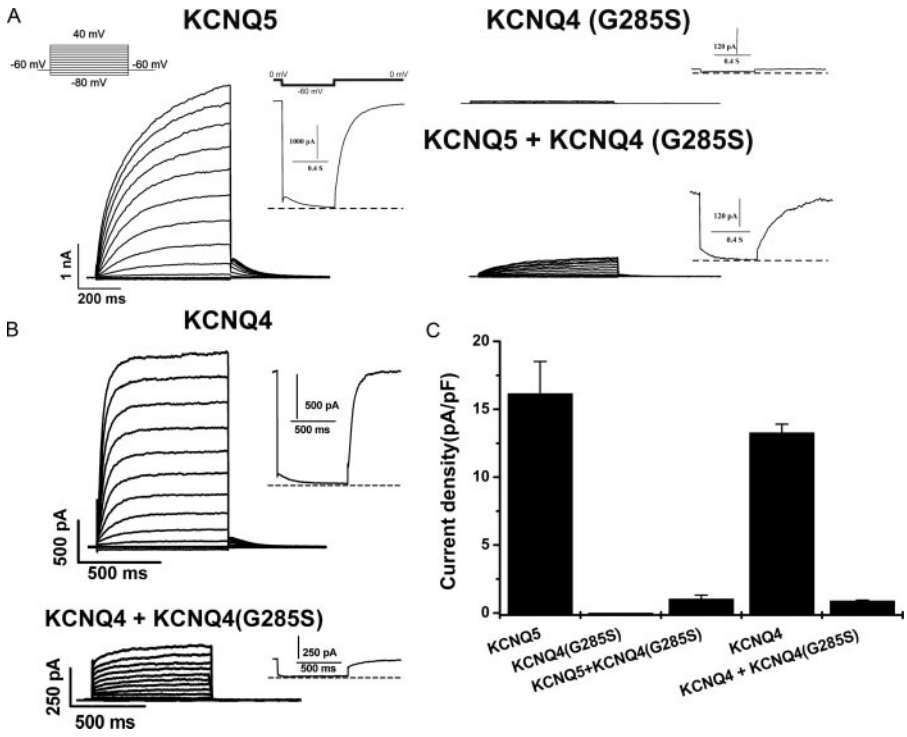

FIGURE 5. **The KCNQ4 (G285S) pore mutant indicates functional assembly with KCNQ5.** CHO cells were transfected with wild-type KCNQ5, KCNQ4 (G285S), wild-type KCNQ4, both wild-type KCNQ5 and KCNQ4 (G285S), or both wild-type KCNQ4 and KCNQ4 (G285S) and studied under perforated patch voltage clamp. *A* and *B*, shown are representative currents from the indicated transfections either using a traditional or "classic" M current protocol (depicted in the *insets*). *C*, *bars* show summarized current densities from the five groups of cells. The KCNQ current was measured as the amplitude of the time-dependent relaxation at −60 mV. *pF*, picofarad.

type and G285S mutant KCNQ4 channels that was not significantly different (supplemental Fig. S1).

As before, expression of KCNQ5 homomers was high (16.2 ± 2.3 pA/picofarad, $n = 19$). In cells co-transfected with KCNQ4 (G285S) and KCNQ5 in equal amounts of cDNA, the currents were only very small (1.03 ± 0.29 pA/picofarad, $n = 18$) as were those co-transfected with wild-type KCNQ4 and KCNQ4 (G285S) (0.89 ± 0.06 pA/picofarad, $n = 12$). If KCNQ4 and KCNQ5 do not co-assemble, then we predict a current density from co-expression of KCNQ4 (G285S) and KCNQ5 to be one-half that from KCNQ5 alone because the currents would arise from the one-half KCNQ5 cDNA transfected that solely produced functional channels. On the other hand, if the two types of subunits do co-assemble, then the four of five populations of tetramers containing at least one KCNQ4 (G285S) would be silent, and only the minor population of KCNQ5 homomers would produce currents. For equal abundance of the two types of subunits, the binomial distribution predicts that population to be 6.25% of the total. In fact, the cells co-expressing KCNQ4 (G285S) + KCNQ5 subunits yielded a current density 6.36% that of cells expressing only KCNQ5, and our control test of wild-type KCNQ4 co-expressed with KCNQ4 (G285S) similarly yielded a current density 6.7% that of KCNQ4 alone. Both results are in excellent agreement with the prediction expected from co-assembled subunits. Thus, we conclude that KCNQ4 and KCNQ5 indeed do co-assemble into channel tetramers in accord with their association indicated by the TIRF/FRET data.

DISCUSSION

KCNQ subunits assemble to form a variety of homomeric and heteromeric channels with diverse physiological functions among tissues. Here we consider only the assembly of the KCNQ pore-forming α-subunits and not the family of KCNE β-subunits that assemble with at least KCNQ1 and KCNQ4, modifying their function in diverse ways (45, 46). For the KCNQ1 and KCNQ4 subunits that are robustly expressed as homomers in both native and heterologous systems, the function seems to be K^+ transport rather than electrical signaling. Thus, inherited mutations in those channels produce inherited syndromes manifested by impaired K^+ transport mostly in several epithelial tissues (47, 48). On the other hand, the major physiological role of KCNQ2, KCNQ3, KCNQ5, and KCNQ1/KCNE1 heteromers is electrical control of neuronal firing and cardiac pacemaking with these subunits nearly always expressed as heteromeric channels in excitable cells (39, 45, 49). Consequently inherited mutations of those subunits give rise to a number of syndromes of epileptic seizures and cardiac arrhythmias (7, 50, 51). Channels from these different subunits possess very different characteristics of many types, including unitary conductance and open probability; sensitivity to phosphoinositides, Ca^{2+}/calmodulin, and protein kinases; and interactions with protein kinase A-anchoring proteins (15, 17, 19, 52–55). Thus, the selective expression of subunits in different cells likely represents a vigorous transcriptional mechanism to guide cellular function in accord with the particular functional agenda of the cell, providing the rationale for scrutiny of the allowed KCNQ subunit combinations.

This study had several aims. The first was to determine further the allowed heteromeric assembly of KCNQ channels. Consistent with previous work, our TIRF/FRET results indicate that KCNQ1 and KCNQ4 and that KCNQ2 and KCNQ5 do not interact. The data further suggest KCNQ4 to be unexpectedly promiscuous, interacting with both KCNQ3 and KCNQ5. The former is congruent with the data of Kubisch *et al.* (8) who used a KCNQ3 pore mutant to show functional assembly with KCNQ4. Here the functionality of KCNQ4/5 heteromers was confirmed by use of a similar KCNQ4 dominant-negative pore mutant.

KCNQ4 has been shown to broadly localize to the neural auditory axis, including the hair cells of the cochlea, the vestib-

ular organs, several auditory and sensory nuclei of the brainstem, and other dopaminergic brain regions (1, 9, 56). Because KCNQ2 and KCNQ3 subunits also localize to these regions (6, 57) and because KCNQ3 has also been shown to functionally co-assemble with KCNQ5 (22, 58), this raises the possibility of KCNQ3/4/5 heteromers in addition to the KCNQ2/3/5 heteromers suggested to underlie some M channels in sympathetic (3) and sensory (59) ganglia. Clearly the spectrum of possible combinations of "M-type" channels is highly diversified. The allowed assembly of KCNQ3/4 subunits is in accord with the expression of both RNA transcripts in the cochlea (8) and with the localization of KCNQ4 subunits to a number of regions the brain (9) that very likely also express KCNQ3. For all the regions of the ear and nervous system that have been shown to contain KCNQ4 subunits, it will now be interesting to look for the presence of KCNQ5 as well. Finally the 40-fold increase in external TEA sensitivity by the T290Y mutation provides further evidence for the role of an aromatic residue in that position for KCNQ channels as for many other K^+ channels. It is unclear whether the sole expression by KCNQ2 of such a residue there serves some physiological purpose or is only happenstance.

Another aim of this study was to determine whether the divergent expression of KCNQ1–5 homomers seen in heterologous expression systems might be due to differential tetramerization of subunits in the membrane. Whereas KCNQ1, KCNQ4, and KCNQ5 homomers yield robust current amplitudes when expressed in oocytes or mammalian cells, those of KCNQ2 and KCNQ3 are much smaller (Ref. 60 and references therein; this study). For KCNQ2, we have shown its low apparent affinity for the phosphoinositides necessary for channel opening (61) to be the origin of small homomeric KCNQ2 currents (53). One explanation for the small homomeric KCNQ3 currents has been impaired tetramerization because of the paucity of salt bridges in critical carboxyl-terminal coiled coil domains (16, 62, 63). Thus, it was possible that the assembly of KCNQ3 monomers in the membrane might be reduced compared with that of the other subunit types, underlying the small KCNQ3 currents. However, the TIRF/FRET data here rule out that possibility as the FRET efficiency between CFP- and YFP-tagged KCNQ3 subunits was no less than that for the others. Indeed we recently have suggested that mechanism to be due to the presence of many dormant KCNQ3 channels in the membrane because of a structurally silent conformation of the channel pore (60). Likewise our analysis of the relative expression of functional channels in the membrane that takes into account maximal open probability and unitary current of the single channel suggests a density for KCNQ4 10-fold greater than that for KCNQ1 or KCNQ2/3 channels (58). Our data here also rule out the greater assembly of KCNQ4 subunits in the membrane as the explanation.

Many recent studies have shown M channels to play pivotal roles in control of neuronal discharge, axonal conduction, neurotransmitter release, and somatic excitability (64–75). These studies are in addition to the seminal link between M current and syndromes of human epilepsy (7, 76–79). Furthermore it is now clear that M channel activity is intimately involved in pain sensation and response as well as control of visceral organs at the level of several different types of sensory neurons (59, 80, 81). Thus, the selection of which subunit assembly types are expressed in any given neuron will have powerful effects on physiological function throughout the body. We look forward to a further understanding of the expression patterns of KCNQ subunits in the diverse tissues of the body and to the elucidation of the functional link between membrane excitability, cellular function, and regulatory control over KCNQ channel combinatorial expression.

Acknowledgments—We thank Giselle Fernandez, S. Katherine Boyd, and Pamela Martin for expert technical assistance.

REFERENCES

1. Hadley, J. K., Passmore, G. M., Tatulian, L., Al-Qatari, M., Ye, F., Wickenden, A. D., and Brown, D. A. (2003) *J. Neurosci.* **23,** 5012–5019
2. Shah, M. M., Mistry, M., Marsh, S. J., Brown, D. A., and Delmas, P. (2002) *J. Physiol.* **544,** 29–37
3. Schroeder, B. C., Hechenberger, M., Weinreich, F., Kubisch, C., and Jentsch, T. J. (2000) *J. Biol. Chem.* **275,** 24089–24095
4. Shapiro, M. S., Roche, J. P., Kaftan, E. J., Cruzblanca, H., Mackie, K., and Hille, B. (2000) *J. Neurosci.* **20,** 1710–1721
5. Wang, H. S., Pan, Z., Shi, W., Brown, B. S., Wymore, R. S., Cohen, I. S., Dixon, J. E., and McKinnon, D. (1998) *Science* **282,** 1890–1893
6. Cooper, E. C., Harrington, E., Jan, Y. N., and Jan, L. Y. (2001) *J. Neurosci.* **21,** 9529–9540
7. Cooper, E. C., and Jan, L. Y. (2003) *Arch. Neurol.* **60,** 496–500
8. Kubisch, C., Schroeder, B. C., Friedrich, T., Lutjohann, B., El-Amraoui, A., Marlin, S., Petit, C., and Jentsch, T. J. (1999) *Cell* **96,** 437–446
9. Kharkovets, T., Hardelin, J. P., Safieddine, S., Schweizer, M., El-Amraoui, A., Petit, C., and Jentsch, T. J. (2000) *Proc. Natl. Acad. Sci. U. S. A.* **97,** 4333–4338
10. Nicolas, M., Dememes, D., Martin, A., Kupershmidt, S., and Barhanin, J. (2001) *Hear. Res.* **153,** 132–145
11. Robbins, J. (2001) *Pharmacol. Ther.* **90,** 1–19
12. Etxeberria, A., Santana-Castro, I., Regalado, M. P., Aivar, P., and Villarroel, A. (2004) *J. Neurosci.* **24,** 9146–9152
13. Schroeder, B. C., Kubisch, C., Stein, V., and Jentsch, T. J. (1998) *Nature* **396,** 687–690
14. Yang, W. P., Levesque, P. C., Little, W. A., Conder, M. L., Ramakrishnan, P., Neubauer, M. G., and Blanar, M. A. (1998) *J. Biol. Chem.* **273,** 19419–19423
15. Gamper, N., Stockand, J. D., and Shapiro, M. S. (2003) *J. Neurosci.* **23,** 84–95
16. Schwake, M., Athanasiadu, D., Beimgraben, C., Blanz, J., Beck, C., Jentsch, T. J., Saftig, P., and Friedrich, T. (2006) *J. Neurosci.* **26,** 3757–3766
17. Gamper, N., Li, Y., and Shapiro, M. S. (2005) *Mol. Biol. Cell* **16,** 3538–3551
18. Hoshi, N., Zhang, J. S., Omaki, M., Takeuchi, T., Yokoyama, S., Wanaverbecq, N., Langeberg, L. K., Yoneda, Y., Scott, J. D., Brown, D. A., and Higashida, H. (2003) *Nat. Neurosci.* **6,** 564–571
19. Hoshi, N., Langeberg, L. K., and Scott, J. D. (2005) *Nat. Cell Biol.* **7,** 1066–1073
20. Chen, L., Kurokawa, J., and Kass, R. S. (2005) *J. Biol. Chem.* **280,** 31347–31352
21. Kurokawa, J., Motoike, H. K., Rao, J., and Kass, R. S. (2004) *Proc. Natl. Acad. Sci. U. S. A.* **101,** 16374–16378
22. Wickenden, A. D., Zou, A., Wagoner, P. K., and Jegla, T. (2001) *Br. J. Pharmacol.* **132,** 381–384
23. Lerche, C., Scherer, C. R., Seebohm, G., Derst, C., Wei, A. D., Busch, A. E., and Steinmeyer, K. (2000) *J. Biol. Chem.* **275,** 22395–22400
24. Schwake, M., Jentsch, T. J., and Friedrich, T. (2003) *EMBO Rep.* **4,** 76–81
25. Gordon, G. W., Berry, G., Liang, X. H., Levine, B., and Herman, B. (1998) *Biophys. J.* **74,** 2702–2713
26. Sekar, R. B., and Periasamy, A. (2003) *J. Cell Biol.* **160,** 629–633
27. Kerschensteiner, D., Soto, F., and Stocker, M. (2005) *Proc. Natl. Acad. Sci. U. S. A* **102,** 6160–6165

28. Zheng, J., and Zagotta, W. N. (2004) *Neuron* **42,** 411–421
29. Amiri, H., Schultz, G., and Schaefer, M. (2003) *Cell Calcium* **33,** 463–470
30. Zheng, J., Trudeau, M. C., and Zagotta, W. N. (2002) *Neuron* **36,** 891–896
31. Axelrod, D. (2003) *Methods Enzymol.* **361,** 1–33
32. Fowler, C. E., Aryal, P., Suen, K. F., and Slesinger, P. A. (2007) *J. Physiol.* **580,** 51–65
33. Gamper, N., Stockand, J. D., and Shapiro, M. S. (2005) *J. Pharmacol. Toxicol. Methods* **51,** 177–185
34. Centonze, V. E., Sun, M., Masuda, A., Gerritsen, H., and Herman, B. (2003) *Methods Enzymol.* **360,** 542–560
35. Steyer, J. A., and Almers, W. (2001) *Nat. Rev. Mol. Cell Biol.* **2,** 268–275
36. Staruschenko, A., Medina, J. L., Patel, P., Shapiro, M. S., Booth, R. E., and Stockand, J. D. (2004) *J. Biol. Chem.* **279,** 27729–27734
37. Bal, M., Zaika, O., Martin, P., and Shapiro, M. S. (2008) *J. Physiol.* **586,** 2307–2320
38. Schwake, M., Pusch, M., Kharkovets, T., and Jentsch, T. J. (2000) *J. Biol. Chem.* **275,** 13343–13348
39. Cooper, E. C., Aldape, K. D., Abosch, A., Barbaro, N. M., Berger, M. S., Peacock, W. S., Jan, Y. N., and Jan, L. Y. (2000) *Proc. Natl. Acad. Sci. U. S. A* **97,** 4914–4919
40. Hadley, J. K., Noda, M., Selyanko, A. A., Wood, I. C., Abogadie, F. C., and Brown, D. A. (2000) *Br. J. Pharmacol.* **129,** 413–415
41. Heginbotham, L., and MacKinnon, R. (1992) *Neuron* **8,** 483–491
42. MacKinnon, R., and Yellen, G. (1990) *Science* **250,** 276–279
43. Kavanaugh, M. P., Hurst, R. S., Yakel, J., Varnum, M. D., Adelman, J. P., and North, R. A. (1992) *Neuron* **8,** 493–497
44. Liman, E. R., Tytgat, J., and Hess, P. (1992) *Neuron* **9,** 861–871
45. Jespersen, T., Grunnet, M., and Olesen, S. P. (2005) *Physiology* (*Bethesda*) **20,** 408–416
46. Strutz-Seebohm, N., Seebohm, G., Fedorenko, O., Baltaev, R., Engel, J., Knirsch, M., and Lang, F. (2006) *Cell Physiol. Biochem.* **18,** 57–66
47. Jentsch, T. J. (2000) *Nat. Rev. Neurosci.* **1,** 21–30
48. Peroz, D., Rodriguez, N., Choveau, F., Baro, I., Merot, J., and Loussouarn, G. (2008) *J. Physiol.* **586,** 1785–1789
49. Roche, J. P., Westenbroek, R., Sorom, A. J., Hille, B., Mackie, K., and Shapiro, M. S. (2002) *Br. J. Pharmacol.* **137,** 1173–1186
50. Maljevic, S., Wuttke, T. V., and Lerche, H. (2008) *J. Physiol.* **586,** 1791–1801
51. Loussouarn, G., Baro, I., and Escande, D. (2006) *Methods Mol. Biol.* **337,** 167–183
52. Delmas, P., and Brown, D. A. (2005) *Nat. Rev. Neurosci.* **6,** 850–862
53. Li, Y., Gamper, N., Hilgemann, D. W., and Shapiro, M. S. (2005) *J. Neurosci.* **25,** 9825–9835
54. Li, Y., Gamper, N., and Shapiro, M. S. (2004) *J. Neurosci.* **24,** 5079–5090
55. Marx, S. O., and Kurokawa, J. (2006) *Handb. Exp. Pharmacol.* 221–233
56. Hurley, K. M., Gaboyard, S., Zhong, M., Price, S. D., Wooltorton, J. R., Lysakowski, A., and Eatock, R. A. (2006) *J. Neurosci.* **26,** 10253–10269
57. Anantharam, A., Lewis, A., Panaghie, G., Gordon, E., McCrossan, Z. A., Lerner, D. J., and Abbott, G. W. (2003) *J. Biol. Chem.* **278,** 11739–11745
58. Yus-Najera, E., Munoz, A., Salvador, N., Jensen, B. S., Rasmussen, H. B., Defelipe, J., and Villarroel, A. (2003) *Neuroscience* **120,** 353–364
59. Passmore, G. M., Selyanko, A. A., Mistry, M., Al-Qatari, M., Marsh, S. J., Matthews, E. A., Dickenson, A. H., Brown, T. A., Burbidge, S. A., Main, M., and Brown, D. A. (2003) *J. Neurosci.* **23,** 7227–7236
60. Zaika, O., Hernandez, C. C., Bal, M., Tolstykh, G. P., and Shapiro, M. S. (2008) *Biophys. J.*, in press
61. Suh, B. C., and Hille, B. (2007) *J. Physiol.* **582,** 911–916
62. Howard, R. J., Clark, K. A., Holton, J. M., and Minor, D. L., Jr. (2007) *Neuron* **53,** 663–675
63. Nakajo, K., and Kubo, Y. (2008) *J. Physiol.* **586,** 2827–2840
64. Chen, S., and Yaari, Y. (2008) *J. Physiol.* **586,** 1351–1363
65. Peretz, A., Sheinin, A., Yue, C., Degani-Katzav, N., Gibor, G., Nachman, R., Gopin, A., Tam, E., Shabat, D., Yaari, Y., and Attali, B. (2007) *J. Neurophysiol.* **97,** 283–295
66. Piccinin, S., Randall, A. D., and Brown, J. T. (2006) *J. Neurophysiol.* **95,** 3105–3112
67. Vervaeke, K., Gu, N., Agdestein, C., Hu, H., and Storm, J. F. (2006) *J. Physiol.* **576,** 235–256
68. Lawrence, J. J., Saraga, F., Churchill, J. F., Statland, J. M., Travis, K. E., Skinner, F. K., and McBain, C. J. (2006) *J. Neurosci.* **26,** 12325–12338
69. Zaika, O., Lara, L. S., Gamper, N., Hilgemann, D. W., Jaffe, D. B., and Shapiro, M. S. (2006) *J. Physiol.* **575,** 49–67
70. Zaika, O., Tolstykh, G. P., Jaffe, D. B., and Shapiro, M. S. (2007) *J. Neurosci.* **27,** 8914–8926
71. Yue, C., and Yaari, Y. (2006) *J. Neurophysiol.* **95,** 3480–3495
72. Shen, W., Hamilton, S. E., Nathanson, N. M., and Surmeier, D. J. (2005) *J. Neurosci.* **25,** 7449–7458
73. Gu, N., Vervaeke, K., Hu, H., and Storm, J. F. (2005) *J. Physiol.* **566,** 689–715
74. Devaux, J. J., Kleopa, K. A., Cooper, E. C., and Scherer, S. S. (2004) *J. Neurosci.* **24,** 1236–1244
75. Martire, M., Castaldo, P., D'Amico, M., Preziosi, P., Annunziato, L., and Taglialatela, M. (2004) *J. Neurosci.* **24,** 592–597
76. Coppola, G., Castaldo, P., Miraglia Del Giudice, E., Bellini, G., Galasso, F., Soldovieri, M. V., Anzalone, L., Sferro, C., Annunziato, L., Pascotto, A., and Taglialatela, M. (2003) *Neurology* **61,** 131–134
77. Castaldo, P., del Giudice, E. M., Coppola, G., Pascotto, A., Annunziato, L., and Taglialatela, M. (2002) *J. Neurosci.* **22,** 1–6
78. Lerche, H., Jurkat-Rott, K., and Lehmann-Horn, F. (2001) *Am. J. Med. Genet* **106,** 146–159
79. Biervert, C., Schroeder, B. C., Kubisch, C., Berkovic, S. F., Propping, P., Jentsch, T. J., and Steinlein, O. K. (1998) *Science* **279,** 403–406
80. Wladyka, C. L., Feng, B., Glazebrook, P. A., Schild, J. H., and Kunze, D. L. (2008) *J. Physiol.* **586,** 795–802
81. Wladyka, C. L., and Kunze, D. L. (2006) *J. Physiol.* **575,** 175–189